Chloride ion evokes taste sensation by binding to the extracellular ligand-binding domain of sweet/umami taste receptors

Authors:

Nanako Atsumi[1], Keiko Yasumatsu[2], Yuriko Takashina[3], Chiaki Ito[1], Norihisa Yasui[1], Atsuko Yamashita[1]

Affiliation:

[1]Graduate School of Medicine, Dentistry and Pharmaceutical Sciences, Okayama University, Okayama, Japan, [2]Oral Health Science Center, Tokyo Dental College, Tokyo, [3]Faculty of Pharmaceutical Sciences, Okayama University, Okayama, Japan.

Corresponding author:

Atsuko Yamashita, Graduate School of Medicine, Dentistry and Pharmaceutical Sciences, Okayama University, 1-1-1, Tsushima-naka, Kita-ku, Okayama 600-8530, Japan. Fax: +81-86-251-7974. E-mail: a_yama@okayama-u.ac.jp.

Keywords:

Taste receptor, salt taste, chloride

Abstract

The taste sensation of salt is multifaceted: table salt (NaCl) at low concentrations is perceived as a preferable taste through the salty taste receptor, while that at higher concentrations is perceived as an aversive taste through distinct pathways. In addition, Cl^- is also thought to participate in taste sensation through a currently unknown mechanism. Here we describe a Cl^--ion binding and the response of taste receptor type 1 (T1r), a receptor family composing sweet/umami receptors. The T1r2a/T1r3 heterodimer from medaka fish, an amino-acid taste receptor and the sole T1r member whose structure has been solved, exhibited a specific Cl^--binding in the vicinity of the amino-acid-binding site in the ligand-binding domain (LBD) of T1r3. Notably, the Cl^--binding site is likely conserved among T1r3 from other species, including humans. The Cl^--binding at the site is considered to organize the structures of the amino-acid binding site and heterodimer interface. Indeed, the Cl^--binding was found to induce a conformational change of T1r2a/T1r3LBD at sub-mM to low-mM concentrations in a similar manner to canonical taste substances. In order to address the physiological significance of the Cl^- action on T1r, single fiber responses from mouse taste nerves connected to T1r-expressing taste cells were investigated. As a result, a Cl^- application increased impulse frequencies, which were inhibited by a lingual application of a T1r-specific blocker. These results suggest that the Cl^- evokes taste sensations by binding to T1r, underlying a reported “sweet” taste sensation by table salt at a low concentration.

Significance statement

Salt taste sensation is essential for regulating salt intake and maintaining body fluid volume and concentration. Therefore, in concentrations close to that of body fluid, the sodium ion is perceived as an appealing taste through a specific taste transduction pathway. In this study, we found that a low concentration of chloride ion, a sodium ion counter anion in table salt, is

perceived via the sweet taste transduction pathway mediated by the sweet taste receptor, one of the attractive taste qualities in animals. The chloride perception system discovered in this study could be another attractive pathway for promoting salt intake in an appropriate concentration range.

Introduction

Taste sensation is initiated by a specific interaction between chemicals in foods and taste receptors in taste buds in the oral cavity. In vertebrates, the chemicals is categorized into five basic modalities; sweet, umami, bitter, salty, and sour. This perception occurs via taste receptor recognition that is specific to a group of chemicals representing each taste modality (1). With regard to the salty taste, the preferable taste, around ~ 100 mM concentration of table salt, is evoked by specific interaction between epithelial sodium channel (ENaC) and sodium ion (2). Notably, salt sensation exhibits multifaced properties, suggesting the existence of an adequate concentration range for salt intake to maintain the homeostasis of body fluid concentration. For example, high concentrations of salt over levels perceived as a preferable taste, such as ~ 500 mM, are known to stimulate bitter and sour taste cells and are perceived as an aversive taste (3). Conversely, low concentrations of salt under the "preferable" concentration, such as mM to a hundred mM concentration, are perceived as sweet by human panels (4-6). However, its mechanism has never been extensively pursued. The various impacts of the salt taste sensation indicate the presence of multiple salt detection pathways in taste buds. Moreover, another component of table salt, chloride ion, is thought to participate in taste sensation because of the existence of the "anion effect": the salty taste is most strongly perceived when the counter anion is a chloride ion (7). However, several reports have revealed that chloride ions are perceived by an unknown ENaC-independent pathway (8, 9). Indeed, a recent study indicated that transmembrane channel-like 4 (TMC4) expressed in taste buds involves high-concentration Cl^--perception (10). Nevertheless, no candidate molecules capable of perceiving low or preferable concentrations of Cl^- have been elucidated. Therefore, the complete understanding of salt taste sensation, including the mechanism of chloride ion perception, remains unclear.

Unlike salt taste sensation, those for nutrients such as sugars, amino acids, and

nucleotides are well understood as sweet and umami perception through specific receptor proteins (11-13). Sweet and umami receptors are composed of taste receptor type 1 (T1r) proteins in the class C G protein-coupled receptor family. In humans, the T1r1/T1r3 heterodimer serves as the umami taste receptor and perceives amino acids as L-glutamate and aspartate, and nucleotides. In contrast, the T1r2/T1r3 heterodimer serves as the sweet taste receptor and perceives sugars. Previously, we elucidated the crystallographic structure of the medaka fish T1r2a/T1r3 extracellular ligand-binding domain (LBD) (14), which is currently the sole reported structure of T1rs. In the structure, the amino-acid binding was observed in the middle of the LBD of both T1r2a and T1r3 subunits, consistent with the fact that T1r2a/T1r3 is an amino-acid receptor (15). Furthermore, chloride ion binding was found in the vicinity of the amino-acid binding site in T1r3 (Figure 1A). Thus far, the physiological significance of Cl^--binding for T1rs functions has not been explored. Nevertheless, chloride ions are thought to regulate another receptor in class C GPCRs, metabotropic glutamate receptors (mGluRs), and act as positive modulators for agonist binding (16-19). Under these conditions, the potential effect of Cl^--binding on T1r receptor function is of significant interest.

In this study, we investigated the Cl^- actions on T1rs using structural, biophysical, and physiological analyses. The Cl^-–binding to the LBD was investigated using the medaka fish T1r2a/T1r3LBD, which is amenable to structural and biophysical analyses. Since the Cl^--binding site in T1r3 was conserved across various species, taste nerve recordings from mouse were used to investigate the physiological significance of Cl^-. The results suggest that Cl^- induces the moderate response via T1rs, implying that T1rs are involved in Cl^- perception in taste buds.

Results

Cl^--binding site in T1r3

In the previously reported structure of T1r2a/T1r3LBD crystallized in the presence of NaCl, bound Cl^- was identified based on electron density and binding distances (14). To verify the Cl^--binding, Cl^- in the T1r2a/T1r3LBD crystal was substituted with Br^-, a halogen ion amenable for specific detection by anomalous scattering using a synchrotron light source (Table S1). The diffraction data from the crystal resulted in an anomalous difference Fourier peak at 14.1 σ at the site in the vicinity of the amino-acid binding site in T1r3, where Cl^- was originally bound (Figure 1B, Figure S1A). For further confirmation, the anomalous data of the original crystal containing Cl^- was collected at a long wavelength of 2.7 Å, where the anomalous peak for Cl and several other elements such as Ca or S can be detected (Table S1). The resultant anomalous difference Fourier map showed a peak at the bound Cl^- position, while all the other peaks were observed at the S atoms in the protein (Figure 1C, Figure S1B). These results verify that the site is able to bind halogen ions, likely accommodating Cl^- under physiological conditions.

Cl^- was coordinated at the binding site by the side-chain hydroxyl group of Thr105 and the main-chain amide groups of Gln148 and Ser149 (Figure 1D). These main-chain coordinating residues are followed by Ser150, a critical residue for binding amino-acid ligands (14). Furthermore, the loop regions where Thr105 and the Gln148-Ser150 locate are followed by helices B and C, respectively. These helices are essential structural units at the heterodimer interface (14) (Figure 1A). They are known to reorient upon agonist binding, resulting in conformation rearrangement, likely inducing receptor activation in class C GPCRs (20, 21). In addition, the side-chain hydroxyl group of Ser149, which serves as a cap for the positive helix dipole of helix C, simultaneously functions as a distal ligand for Cl^- coordination. Therefore, the Cl^- binding at this site is important for organizing the structure of

the amino-acid binding site and the heterodimer interface.

The Cl^--binding site observed in the crystal structure is most likely conserved among T1r3s in many different organisms, including humans (Figure 1E). Thr105, the residue that provides the side-chain-coordinating ligand for Cl^--binding, is conserved as either serine or threonine among T1r3s. In addition, the amino-acid sequences surrounding the main-chain-coordinating ligands, Pro44, Gln148, and Ser149, are moderately conserved. Notably, the site structurally corresponds to the Cl^--binding site in the hormone-binding domain of the atrial natriuretic peptide receptor (ANPR) (Figure 1F, G). Although ANPR is not a member of class C GPCR, the hormone-binding domain in ANPR shares a similar structural fold with LBD of T1rs and other class C GPCRs, and bacterial periplasmic-binding proteins (20, 22). Accordingly, the conservation of the structure and the sequence motif at the Cl^--binding site at ANPR is also observed on mGluRs (23). Cl^- is known to positively regulate the peptide hormone binding in ANPR (24), while some of mGluRs are also known to be regulated by Cl^- (16-19). Indeed, Cl^--binding at the site corresponding to that in T1r3 was observed in several mGluR and other class C GPCR structures (25, 26) (Figure 1F, G) and was identified as a potential site responsible for the regulation of L-glutamate binding in mGluRs (18). These results strongly imply the possibility that Cl^- has some actions on T1r receptor functions.

In contrast, conservation at the Thr105 position was not observed among T1r1 and T1r2 (Figure 1E). Evidently, no significant anomalous peak derived from Br^-- or Cl^--binding was observed in the crystal structure at the corresponding site in T1r2a (Figure 1B, C). His100 in T1r2a, which corresponds to Thr105 in T1r3, adopted a significantly different side-chain conformation from that of Thr105 in T1r3 (Figure S1C). Therefore, T1r1 and T1r2's ability to bind Cl^- is unlikely.

In addition to the Cl^--binding site discussed above, the Br^--substituted crystal

exhibited an anomalous peak at 8.5 σ in T1r2a, at a position close to the Lys265 side-chain ε-amino group (Figure 1B, Figure S1D). Nevertheless, Cl^--binding was not observed in the original Cl^--contained crystal. This is further confirmed by the absence of an anomalous peak at this position in the data collected at 2.7 Å (Figure 1C, Figure S1E). Therefore, the site might have the ability to bind anions such as Br^- or larger; but be not specific to Cl^-. In human T1r1, the residue corresponding to Lys265, Arg277, was suggested as a critical residue for activities of inosine monophosphate, an umami enhancer (27).

Cl^--binding properties in T1r2a/T1r3LBD

To investigate the Cl^- actions on T1r functions, we first examined the properties of the Cl^-–binding to medaka T1r2a/T1r3LBD using various biophysical techniques. For this purpose, the purified T1r2a/T1r3LBD was subjected to differential scanning fluorimetry (DSF), which we previously used for the amino-acid binding analysis (28). In order to prepare a Cl^--free condition, Cl^- in the sample was substituted with gluconate, as it is unlikely accommodated in the Cl^--site due to its much larger size. We also confirmed that gluconate does not serve as an orthosteric ligand (*i.e.*, a taste substance) for T1r2a/T1r3LBD (Figure S2A).

The addition of Cl^- to the Cl^--free T1r2a/T1r3LBD sample resulted in thermal stabilization of the protein (Figure 2A), which is indicative of Cl^- binding to the protein. The apparent K_d value for Cl^- estimated by the melting temperatures (T_m) at various Cl^--concentrations was ~110 μM (Figure 2B, Table 1). The Cl^--dependent thermal stabilization was confirmed by the fluorescence-detection size-exclusion chromatography-based thermostability (FSEC-TS) assay (29) (Figure 2C, Table 1). However, the Cl^--dependent stabilization was not observed on T1r2a/T1r3 with the Cl^--site mutation, T105A in T1r3. In the case of this mutant, the T_m values for both in the presence and absence of Cl^- was similar to that the values obtained for the wild-type protein in the absence of Cl^-, as determined by

both FSEC-TS and DSF (Figure 2C, Figure S2B, Table 1). These results indicate that the Cl^- effect attributed to the identical site where the Cl^--binding was observed in the crystal structure of T1r3.

In the next place, we examined a consequence of the Cl^--binding to T1r2a/T1r3LBD by Förster resonance energy transfer (FRET) using the fluorescent protein-fused sample. Class C GPCRs commonly exhibit agonist-induced conformational changes of LBD, such as the dimer rearrangement, which is essential for receptor activation and signaling (20, 21, 30, 31). Consistent with this, we previously reported that T1r2a/T1r3LBD shows conformational change concomitant with the binding of amino acids, which can be detected as the increase of FRET intensities (32). Notably, the addition of Cl^- to the fluorescent protein-fused T1r2a/T1r3LBD also increased FRET intensities, similar to amino acids (Figure 2D). The EC_{50} for Cl^--induced FRET signal change was determined as ~ 1 mM (Table 1). It should be noted that both DSF and FRET estimations have some degree of error: the former produced slightly lower values than the latter, particularly in the case of weak affinities in the mM concentration range (28). As such, although the EC_{50} value determined by FRET was slightly higher than the apparent K_d value of Cl^-determined by DSF, the two are most likely relevant. Therefore, these results suggest that the Cl^- binding to T1r2a/T1r3LBD induces the conformational rearrangement of T1r2a/T1r3LBD in a similar manner to its agonist amino-acid. Nevertheless, the extent of the FRET change induced by Cl^- was smaller compared to changes induced by amino acids: the FRET index change induced by Cl^- at saturation was estimated as 0.12, while that by L-glutamine at a saturated concentration (1 mM) with the same protein sample was observed as 0.21. Therefore, the results suggest that the extent of the conformational change induced by Cl^- is smaller than the change induced by amino acids.

In addition to the Cl^--binding effect, the Cl^- effect on amino-acid binding to

T1r2a/T1r3LBD was investigated by FRET and isothermal calorimetry (ITC). The K_d values for L-glutamine binding determined by ITC, as well as the EC_{50} values and the other parameters for L-glutamine-induced conformational change determined by FRET, did not differ in the presence and absence of Cl^- (Figure 2E, Figure S2C, 2D, and Table 1). These results indicated that the Cl^--binding had no significant effect on the binding of L-glutamine, a representative taste substance, at least for T1r2a/T1r3LBD from medaka fish.

Taste response to Cl^- through T1rs in mouse

The biophysical studies on T1r2a/T1r3LBD from medaka fish suggested that Cl^- binding to T1r3LBD induces a conformational change similar to that of an agonist without affecting agonist binding. As described above, the Cl^--binding site is likely conserved among T1r3 in various species, such as those in mammals. Therefore, we analyzed single fiber responses from mouse taste nerves to investigate the physiological effect of Cl^- on taste perception. While conventional cell-based receptor assay systems are affected by changes in extracellular ionic components, the application of various solutions to the taste pore side of the taste buds, which are projected to taste nerve systems, are transduced exclusively as “taste” signals, without inducing the other cellular responses derived from the ionic component changes in the surrounding environment.

We first identified a nerve fiber that connects to T1r-expressing taste cells, as evidenced by responses to T1r agonists such as sugars and amino acids, which were inhibited by gurmarin (Gur), a T1r-specific blocker (33-36). Remarkably, the fiber also exhibited responses indued by applying Cl^-, which was added as a form of NMDG-Cl devoid of the known salty taste stimulant, sodium ion (Figure 3A, top and middle rows). Cl^--induced impulse frequencies from the nerve increased in a concentration-dependent manner (Figure 3B). The responses to NMDG-Cl, NaCl, and KCl in the same concentrations did not differ

220 significantly (repeated measures ANOVA, $P > 0.05$), confirming that the observed responses
221 were attributed to Cl^-. All the responses to Cl^-, regardless of the kinds of counter anions,
222 significantly decreased by lingual treatment of Gur (Figure 3B, repeated measures ANOVA:
223 $F_{(1, 42)} = 56.65$, $P < 0.001$ for NMDG-Cl; $F_{(1, 50)} = 24.78$, $P < 0.001$ for NaCl; $F_{(1, 45)} = 35.72$,
224 $P < 0.001$ for KCl). The results indicate that the observed Cl^--dependent responses were
225 mediated by T1r. Notably, the Cl^--concentration range that induced nerve responses was
226 lower than the "preferable" salty taste perceived by ENaC when applied as the NaCl form, but
227 are consistent with those for Cl^--binding and Cl^--induced conformational change observed on
228 T1r2a/T1r3LBD (Table 1), and those perceived as "sweet" by the human panel test for salt
229 tasting (4-6). These results suggested that a low concentration of Cl^- is perceived as a "sweet"
230 taste via T1r. Although the responses induced by known taste substances for T1rs, such as
231 sugars and amino acids, range from tens to hundreds of impulse frequencies per ten seconds,
232 the maximum response level induced by Cl^- was low, ~10 per ten seconds (Figure 3B).
233 According to our observations, Cl^- likely produces a "light" taste sensation when compared to
234 other known taste substances.

235 In order to examine the physiological interaction between a "canonical" taste
236 substance for T1r and Cl^-, we recorded responses to 20 mM L-glutamine or 100 mM sucrose,
237 which induces responses greater than baseline but less than maximum, with or without
238 NMDG-Cl from the same T1r-connecting single fibers (Figure 3A). As shown in Figure3C,
239 the response to L-glutamine or sucrose significantly increased by adding 10 mM NMDG-Cl
240 (paired *t*-test, $t2 = 7.56$, $p = 0.017$ for L-glutamine; $t2 = 5.05$, $p = 0.037$ for sucrose). We
241 confirmed that these responses had been suppressed by a lingual treatment of Gur in the
242 presence ($t2 = 6.73$, $p = 0.021$ for L-glutamine; $t2 = 8.80$, $p = 0.013$ for sucrose) or absence ($t2$
243 $= 8.32$, $p = 0.014$ for L-glutamine; $t2 = 11.72$, $p = 0.007$ for sucrose) of NMDG-Cl to a similar
244 extent. Moreover, the responses to the mixtures did not differ significantly from the

summation of the responses to each solution ($t2 = 2.34$, $p = 0.145$ for L-glutamine; $t2 = 2.31$, $p = 0.147$ for sucrose). The results indicate that the perception of Cl^- and a "canonical" taste substance, such as amino acids and sugars, by T1r is additive and not synergistic.

Discussion

The existence of Cl^- perception through the taste sensory system has long been presumed. However, its molecular basis has not been well-elucidated. In this study, we found that Cl^- specifically interacts with the LBD in T1r3, a common component of sweet and umami taste receptors, and induces a conformational change in the receptor's LBD region. The findings also suggest that Cl^-–binding to T1r in taste cells is transmitted to the sweet taste nervous system, likely resulting in light taste sensation. Since T1rs are conserved across vertebrates and the Cl^-–binding site is likely conserved among T1r3 in various organisms, T1r-mediated Cl^-–perception might be common in many animals, including humans. Evidently, the concentration range for the Cl^--induced conformational change of medaka T1r2a/T1r3LBD and increase of murine sweet nerve impulses observed in this study are consistent with the NaCl concentration perceived as "sweet" by humans (4-6). Furthermore, the sweet sensation induced by NaCl was reportedly suppressed by topical application of *Gymnema sylvestre* (5), which contains Gymnemic acids, which are specific inhibitors for human sweet taste receptor T1r2/T1r3 (37). In addition, Roebber *et al.* reported that Cl^- detection in taste buds is mediated by type 2 cells (9), in which T1rs expression has been found to occur. Overall, these results are consistent with the involvement of T1rs in the Cl^--taste perception. These findings are also consistent with an earlier hypothesis that dilute NaCl contains a sweet stimulus that interacts with the same receptor molecules as sucrose, proposed by Bartoshuk and colleagues in the '70s (5).

Salt taste sensation is an essential physiological process that regulates salt intake to

maintain the body fluid volume and concentration. In order to achieve this, two distinct pathways for salt taste perception have been reported thus far. In the first pathway for salt concentrations close to those found in body fluids, Na^+ is perceived as an appealing taste to promote salt intake via taste cells that express both the Na^+ receptor ENaC and a purinergic neurotransmission channel CALHM1/3 (38). In the second pathway, high salt concentrations, such as at ~ 500 mM NaCl, trigger aversive responses aimed at avoiding salt intake and are mediated through taste cells for bitter and sour taste transductions (3). In this study, the Cl^--perception at low salt concentrations was found to be achieved via the T1rs-mediating attractive sweet taste transduction system. Since Cl^- is also a component of table salt, this system likely serves as another pathway for attractive salt perception promoting intake. Nomura *et al.* reported the existence of the ENaC-independent salt attraction pathway, which is attenuated by CALHM3 knockout (38). Since T1r-induced taste cell signaling is transmitted by CALHM1/3 (39), the T1r-mediated Cl^--perception is consistent with the previous observation and thus might underlie the reported ENaC-independent salt attraction pathway.

Salt taste perception and natriuresis are critical physiological processes that regulate sodium intake and excretion to maintain body fluid homeostasis. Remarkably, both processes use the counter anion Cl^- to regulate the molecular functions of the receptors, T1rs and ANPRs, which share a similar extracellular protein architecture with a conserved Cl^--binding site. In the case of ANPR and mGluRs, positive allosteric modulations for agonist binding have been observed (16-19, 24). In the case of T1rs, however, Cl^--binding induces receptor responses both independently and additively to agonists (taste substances), while no significant enhancement of taste substance-binding by Cl^- was observed. As T1r3 is a common subunit of both sweet and umami taste receptors that respond to different taste substances, the physiological significance of the agonist binding at the orthosteric site in T1r3, near the Cl^- site, is currently unknown. Nevertheless, considering that the extent of the Cl^-

-dependent enhancement observed in mGluRs varies among different subtypes (18, 19), the Cl^- actions on T1rs of other subtypes or from other organisms could be varied and are yet to be examined in the future.

Materials and methods

Crystallography

The L-glutamine-bound T1r2a/T1r3LBD crystals, in complex with a crystallization chaperone Fab16A, were prepared in the presence of NaCl as described (14). For the preparation of the Br^--substituted crystals, the obtained crystals were soaked in a mother liquor consisting of 100 mM MES-Tris, pH 6.0, 50 mM NaBr, 17% PEG1500, 5% PEG400, 5 mM L-glutamine, 2 mM $CaCl_2$, cryoprotected by gradually increasing the concentration of glycerol to 10%, incubated for 2 hours, and flash-frozen.

The X-ray diffraction data were collected at the SPring-8 beamline BL41XU using a PILATUS6M detector (DECTRIS) at wavelength 0.9194 Å or at the Photon Factory beamline BL-1A using an EIGER X4M detector (DECTRIS) at wavelength 2.7 Å. The data were processed with XDS (40). The phases for anomalous difference Fourier map calculation were obtained by molecular replacement methods with the program PHASER (41), using the structures of a single unit of the mfT1r2a-3LBD-Fab16A complex (PDB ID: 5X2M) as the search model.

Differential scanning fluorimetry

Differential scanning fluorimetry was performed as previously described (28). The purified mfT1R2a/3LBD heterodimer protein was prepared (32) and dialyzed with buffer A (20 mM HEPES-NaOH, 300 mM sodium gluconate, pH 7.5) to remove Cl^-.1 μg of the dialyzed protein sample was mixed with Protein Thermal Shift Dye (Applied Biosystems) and 0.003 $^-$

10 mM NaCl in 20 μL of buffer A. The mixture solutions were then loaded to a MicroAmpR Fast Optical 48-Well Reaction Plate (Applied Biosystems). Fluorescent intensities were measured by the StepOne Real-Time PCR System (Applied Biosystems) while the temperature raised from 25 °C to 99 °C with a velocity of 0.022 °C/sec. For detection, the reporter and quencher were set as "ROX" and "none," respectively. The apparent melting transition temperature (T_m) was determined using the maximum of the derivatives of the melt curve (dFluorescence/dT) by Protein Thermal Shift Software version 1.3 (Applied Biosystems). The apparent dissociation constant ($K_{d\text{-app}}$) for Cl^- derived from the T_m values at different NaCl concentrations was estimated using a thermodynamic model proposed by Schellman (42) as described (28).

Förster resonance energy transfer (FRET)

FRET analysis was performed as previously described (14, 32). For the Cl^--titration, the purified T1r2aLBD-Cerulean and T1r3LBD-Venus heterodimer was dialyzed against buffer A. Afterward, the sample was incubated in the presence of 0.001–10 mM NaCl at 4 °C overnight. For L-glutamine titration in the presence or absence of Cl^-, the protein solution was dialyzed with buffer B (20 mM HEPES-Tris, 300 mM NaCl, pH 7.5) or buffer C (20 mM HEPES-Tris, 300 mM sodium gluconate, pH 7.5) to prepare the conditions with or without Cl^-, respectively. Then, the sample was incubated in the presence of 0.01–1000 μM L-glutamine at 4 °C overnight. The fluorescence spectra were recorded at 298 K with a FluoroMax4 spectrofluorometer (Horiba). The sample was excited at 433 nm, and FRET was detected by the emission at 526 nm. The emission at 475 nm was also recorded for the FRET index calculation. The FRET index (Intensity at 526 nm/Intensity at 475 nm) was plotted against the Cl^- or L-glutamine concentration and the titration curves were fitted to the Hill equation by using KaleidaGraph (Synergy Software) or ORIGIN (OriginLab).

Isothermal calorimetry

In order to prepare the conditions with or without Cl^-, the purified mfT1R2a/3LBD heterodimer protein was dialyzed with buffers B or C, respectively. The dialyzed protein solution (~50 μM) was then loaded into the sample cell in iTC200 (GE Healthcare) after the removal of insoluble materials by centrifugation (10,000×*g*, 15 min, 277 K). The titration was performed by injecting 2 μL of 400 μM L-glutamine at intervals of 120 s at 298 K. The thermograms and the binding isotherms were analyzed with Origin software, assuming one set of binding sites for fitting.

Fluorescence-detection size-exclusion chromatography-based thermostability assay (FSEC-TS)

A T1r3-T105A mutation was introduced in the vector pAc_mfT1r3L (43) by PCR. The mutant expression vector was co-introduced with pAc_mft1r2aL (43) to Drosophila S2 cells to establish a stable high-expression clone cell as previously described (43). The wild-type T1r2a/T1r3LBD and mutant T1r2a/T1r3-105A-LBD proteins were expressed and purified as previously described (32) with several modifications as listed below. After the protein binding to ANTI-FLAG M2 affinity gel, the resin was washed with either buffer D (20 mM HEPES-NaOH, 0.3 M NaCl, 2 mM $CaCl_2$, 5 mM L-Gln, pH 7.5) or buffer E (20 mM HEPES-NaOH, 0.3 M Na gluconate, 2 mM Ca gluconate, 5 mM L-Gln, pH 7.5). Then, the protein was eluted with 100 μg/mL FLAG peptide in buffer D or E.

The protein solutions (50 μg/mL) in buffer D or E were incubated at 4 °C, 37 °C, 50 °C, 70 °C, or 90 °C at 2 hours. Subsequently, the samples were loaded on an SEC-5 column, 500 Å, 4.6 × 300 mm (Agilent) connected to a Prominence HPLC system (Shimadzu), using buffer D or E as a running buffer at a flow rate of 0.3 ml min^{-1}. The elution profiles

were detected with an RF-20A fluorometer (Shimadzu), using excitation and emission wavelengths of 280 and 340 nm for the detection of intrinsic tryptophan fluorescence.

The residual ratio after incubation at each temperature was estimated using the fluorescence intensity at the elution peak, which corresponded to the T1rLBD dimer, *i.e.*, the peak height at ~11.6 min. The values were normalized to the intensity of the sample incubated at 4 °C as 1. In order to estimate the apparent melting temperature ($T_{\text{m-app}}$) of the sample, the values of residual ratio at each temperature were fitted to the Gibbs-Helmholtz equation transformed as shown below (assuming that the sample protein is under equilibrium between a folding and unfolding state under each condition):

$$Residual\ ratio = 1 - \frac{1}{1 + exp\left[-\frac{\Delta H\left(1 + \frac{T}{T_{m-app}}\right) - \Delta C_P\left\{\left(T_{m-app} - \mathrm{T}\right) + Tln\left(\frac{T}{T_{m-app}}\right)\right\}}{RT}\right]}$$

where ΔH and ΔC_{p} are the enthalpy and heat capacity change of unfolding, respectively; T is the temperature of the sample incubation; R is the gas constant. The fittings were performed with KaleidaGraph (Synergy Software), with ΔH, ΔC_{p}, and $T_{\text{m-app}}$ are set as valuables.

Single fiber recording from mouse chorda tympani (CT) nerve

The subjects were 5 adult male C57BL/6JCrj mice (Charles River Japan, Tokyo, Japan) which were maintained on a 12/12-h light/dark cycle and fed standard rodent chow. The animals were 8–20 weeks of age, ranging in weight from 20 to 30 g. The mice were anesthetized with an injection of sodium pentobarbital (40–50 mg/kg ip) and maintained at a surgical level of anaesthesia, with additional injections (8–10 mg/kg ip every hour). Under anaesthesia, each mouse was fixed in the supine position with a head holder, and the trachea cannulated. The right CT nerve was dissected, free from surrounding tissues, after the removal of the pterygoid muscle and cut at the point of its entry to the tympanic bulla. A single or a few nerve fibers were teased apart with a pair of needles and lifted onto an Ag-AgCl electrode,

and an indifferent electrode was placed in nearby tissue. Their neural activities were amplified (K-1; Iyodenshikagaku, Nagoya, Japan) and recorded on a computer using a PowerLab system (PowerLab/sp4; AD Instruments, Bella Vista, NSW, Australia). For taste stimulation of fungiform papillae, the anterior half of the tongue was enclosed in a flow chamber. Taste solutions or rinses (distilled water) (~24 °C) were delivered to the tongue by gravity flow at the same flow rate (~0.1 ml s^{-1}). For data analysis, we used the net average frequency for 10 sec after the stimulus onset, which was obtained by subtracting the spontaneous frequency for the 10 sec duration before stimulation from after stimulation. In the initial survey to identify a nerve fiber connecting to T1r-expressing cells, test stimuli such as 100 mM NaCl, 10 mM HCl, 500 mM sucrose, 100 mM monopotassium glutamate, 20 mM quinine HCl were separately applied. If the fiber responded to sucrose, we applied 10 μM–100 mM NMDG-Cl, NaCl, KCl, or either of 20 mM L-glutamine or 100 mM sucrose with or without 10 mM NMDG-Cl to the tongue. The reagents used were purchased from Wako Pure Chemical Industries (Osaka, Japan; others). In order to block responses via T1r (33-36), each tongue was treated with 30 μg ml^{-1} (~7 μM) gurmarin (Gur) dissolved in 5 mM phosphate buffer (pH 6.8) for 10min in the same manner as described by Ninomiya & Imoto (33). In order to assure to detect responses from T1r-expressing cells, recordings from Gur-insensitive sweet-responsive fibers were defined as those remaining impulse frequencies to 0.5 M sucrose more than 60% following Gur treatment (34), were excluded from the data. At the end of the experiment, animals were killed by the administration of an overdose of the anaesthetic. Repeated measures ANOVA and Student's paired *t*-test were used to statistically evaluate the effects of chemicals.

Acknowledgments

We thank Drs. Kazuya Hasegawa, Nobuhiro Mizuno, Naohiro Matsugaki for help with X-ray data collection; Junya Nitta and Hikaru Ishida for help with protein preparation; Haruo Ogawa for sharing knowledge about ANPR; Yuzo Ninomiya for valuable discussions. The synchrotron radiation experiment at the BL41XU, SPring-8 were performed with approvals of the Japan Synchrotron Radiation Research Institute (JASRI) (Proposal No. 2016B2534). The synchrotron radiation experiment at the BL-1A, Photon Factory was supported by the Platform for Drug Discovery, Informatics, and Structural Life Science (Proposal No. 1264). This work was financially supported by JSPS KAKENHI Grant Numbers JP17H03644, JP18H04621, JP20H03195, JP20H04778, JP21H05524 (to A.Y.) and JP20H03855 (to K.Y.), Mishima Kaiun Memorial Foundation, and the Salt Science Research Foundation (Proposal No. 2039) (to A.Y.).

References

1. A. Taruno *et al.*, Taste transduction and channel synapses in taste buds. *Pflugers Arch* **473**, 3-13 (2021).
2. J. Chandrashekar *et al.*, The cells and peripheral representation of sodium taste in mice. *Nature* **464**, 297-301 (2010).
3. Y. Oka, M. Butnaru, L. von Buchholtz, N. J. Ryba, C. S. Zuker, High salt recruits aversive taste pathways. *Nature* **494**, 472-475 (2013).
4. L. M. Bartoshuk, D. H. McBurney, C. Pfaffmann, Taste of Sodium Chloride Solutions after Adaptation to Sodium Chloride: Implications for the "Water Taste". *Science* **143**, 967-968 (1964).
5. L. M. Bartoshuk, C. Murphy, C. T. Cleveland, Sweet taste of dilute NaCl: psychophysical evidence for a sweet stimulus. *Physiol Behav* **21**, 609-613 (1978).
6. A. V. Cardello, Taste quality changes as a function of salt concentration in single human taste papillae. *Chem Senses* **4**, 1-13 (1979).
7. Q. Ye, G. L. Heck, J. A. DeSimone, The anion paradox in sodium taste reception: resolution by voltage-clamp studies. *Science* **254**, 724-726 (1991).
8. B. C. Lewandowski, S. K. Sukumaran, R. F. Margolskee, A. A. Bachmanov, Amiloride-Insensitive Salt Taste Is Mediated by Two Populations of Type III Taste

Cells with Distinct Transduction Mechanisms. *J Neurosci* **36**, 1942-1953 (2016).

9. J. K. Roebber, S. D. Roper, N. Chaudhari, The Role of the Anion in Salt (NaCl) Detection by Mouse Taste Buds. *J Neurosci* **39**, 6224-6232 (2019).

10. Y. Kasahara *et al.*, TMC4 is a novel chloride channel involved in high-concentration salt taste sensation. *J Physiol Sci* **71**, 23 (2021).

11. G. Nelson *et al.*, Mammalian sweet taste receptors. *Cell* **106**, 381-390 (2001).

12. G. Nelson *et al.*, An amino-acid taste receptor. *Nature* **416**, 199-202 (2002).

13. X. Li *et al.*, Human receptors for sweet and umami taste. *Proc Natl Acad Sci U S A* **99**, 4692-4696 (2002).

14. N. Nuemket *et al.*, Structural basis for perception of diverse chemical substances by T1r taste receptors. *Nat Commun* **8**, 15530 (2017).

15. H. Oike *et al.*, Characterization of ligands for fish taste receptors. *J Neurosci* **27**, 5584-5592 (2007).

16. L. Eriksen, C. Thomsen, [3H]-L-2-amino-4-phosphonobutyrate labels a metabotropic glutamate receptor, mGluR4a. *Br J Pharmacol* **116**, 3279-3287 (1995).

17. D. Kuang, D. R. Hampson, Ion dependence of ligand binding to metabotropic glutamate receptors. *Biochem Biophys Res Commun* **345**, 1-6 (2006).

18. A. S. Tora *et al.*, Allosteric modulation of metabotropic glutamate receptors by chloride ions. *FASEB J* **29**, 4174-4188 (2015).

19. A. S. Tora *et al.*, Chloride ions stabilize the glutamate-induced active state of the metabotropic glutamate receptor 3. *Neuropharmacology* **140**, 275-286 (2018).

20. N. Kunishima *et al.*, Structural basis of glutamate recognition by a dimeric metabotropic glutamate receptor. *Nature* **407**, 971-977 (2000).

21. A. Koehl *et al.*, Structural insights into the activation of metabotropic glutamate receptors. *Nature* **566**, 79-84 (2019).

22. F. van den Akker *et al.*, Structure of the dimerized hormone-binding domain of a guanylyl-cyclase-coupled receptor. *Nature* **406**, 101-104 (2000).

23. H. Ogawa *et al.*, Reversibly bound chloride in the atrial natriuretic peptide receptor hormone-binding domain: possible allosteric regulation and a conserved structural motif for the chloride-binding site. *Protein Sci* **19**, 544-557 (2010).

24. K. S. Misono, Atrial natriuretic factor binding to its receptor is dependent on chloride concentration: A possible feedback-control mechanism in renal salt regulation. *Circ Res* **86**, 1135-1139 (2000).

25. J. A. Monn *et al.*, Synthesis and pharmacological characterization of C4-disubstituted analogs of 1S,2S,5R,6S-2-aminobicyclo[3.1.0]hexane-2,6-dicarboxylate:

identification of a potent, selective metabotropic glutamate receptor agonist and determination of agonist-bound human mGlu2 and mGlu3 amino terminal domain structures. *J Med Chem* **58**, 1776-1794 (2015).

26. C. Zhang *et al.*, Structural basis for regulation of human calcium-sensing receptor by magnesium ions and an unexpected tryptophan derivative co-agonist. *Sci Adv* **2**, e1600241 (2016).

27. F. Zhang *et al.*, Molecular mechanism for the umami taste synergism. *Proc Natl Acad Sci U S A* **105**, 20930-20934 (2008).

28. T. Yoshida *et al.*, Differential scanning fluorimetric analysis of the amino-acid binding to taste receptor using a model receptor protein, the ligand-binding domain of fish T1r2a/T1r3. *PLoS One* **14**, e0218909 (2019).

29. M. Hattori, R. E. Hibbs, E. Gouaux, A fluorescence-detection size-exclusion chromatography-based thermostability assay for membrane protein precrystallization screening. *Structure* **20**, 1293-1299 (2012).

30. S. Lin *et al.*, Structures of Gi-bound metabotropic glutamate receptors mGlu2 and mGlu4. *Nature* **594**, 583-588 (2021).

31. A. Ellaithy, J. Gonzalez-Maeso, D. A. Logothetis, J. Levitz, Structural and Biophysical Mechanisms of Class C G Protein-Coupled Receptor Function. *Trends Biochem Sci* **45**, 1049-1064 (2020).

32. E. Nango *et al.*, Taste substance binding elicits conformational change of taste receptor T1r heterodimer extracellular domains. *Sci Rep* **6**, 25745 (2016).

33. Y. Ninomiya, T. Imoto, Gurmarin inhibition of sweet taste responses in mice. *Am J Physiol* **268**, R1019-1025 (1995).

34. Y. Ninomiya, T. Imoto, T. Sugimura, Sweet taste responses of mouse chorda tympani neurons: existence of gurmarin-sensitive and -insensitive receptor components. *J Neurophysiol* **81**, 3087-3091 (1999).

35. R. F. Margolskee *et al.*, T1R3 and gustducin in gut sense sugars to regulate expression of Na+-glucose cotransporter 1. *Proc Natl Acad Sci U S A* **104**, 15075-15080 (2007).

36. K. Daly *et al.*, Sensing of amino acids by the gut-expressed taste receptor T1R1-T1R3 stimulates CCK secretion. *Am J Physiol Gastrointest Liver Physiol* **304**, G271-282 (2013).

37. K. Sanematsu *et al.*, Molecular mechanisms for sweet-suppressing effect of gymnemic acids. *J Biol Chem* **289**, 25711-25720 (2014).

38. K. Nomura, M. Nakanishi, F. Ishidate, K. Iwata, A. Taruno, All-Electrical Ca(2+)-Independent Signal Transduction Mediates Attractive Sodium Taste in Taste

Buds. *Neuron* **106**, 816-829 e816 (2020).

39. Z. Ma *et al.*, CALHM3 Is Essential for Rapid Ion Channel-Mediated Purinergic Neurotransmission of GPCR-Mediated Tastes. *Neuron* **98**, 547-561 e510 (2018).

40. W. Kabsch, Xds. *Acta Crystallogr D Biol Crystallogr* **66**, 125-132 (2010).

41. A. J. McCoy *et al.*, Phaser crystallographic software. *J Appl Crystallogr* **40**, 658-674 (2007).

42. J. A. Schellman, Macromolecular Binding. *Biopolymers* **14**, 999-1018 (1975).

43. A. Yamashita, E. Nango, Y. Ashikawa, A large-scale expression strategy for multimeric extracellular protein complexes using Drosophila S2 cells and its application to the recombinant expression of heterodimeric ligand-binding domains of taste receptor. *Protein Sci* **26**, 2291-2301 (2017).

44. H. Ogawa, Y. Qiu, C. M. Ogata, K. S. Misono, Crystal structure of hormone-bound atrial natriuretic peptide receptor extracellular domain: rotation mechanism for transmembrane signal transduction. *J Biol Chem* **279**, 28625-28631 (2004).

45. J. A. Monn *et al.*, Synthesis and Pharmacological Characterization of C4-(Thiotriazolyl)-substituted-2-aminobicyclo[3.1.0]hexane-2,6-dicarboxylates. Identification of (1R,2S,4R,5R,6R)-2-Amino-4-(1H-1,2,4-triazol-3-ylsulfanyl)bicyclo[3.1.0]hexane-2,6-dicarboxylic Acid (LY2812223), a Highly Potent, Functionally Selective mGlu2 Receptor Agonist. *J Med Chem* **58**, 7526-7548 (2015).

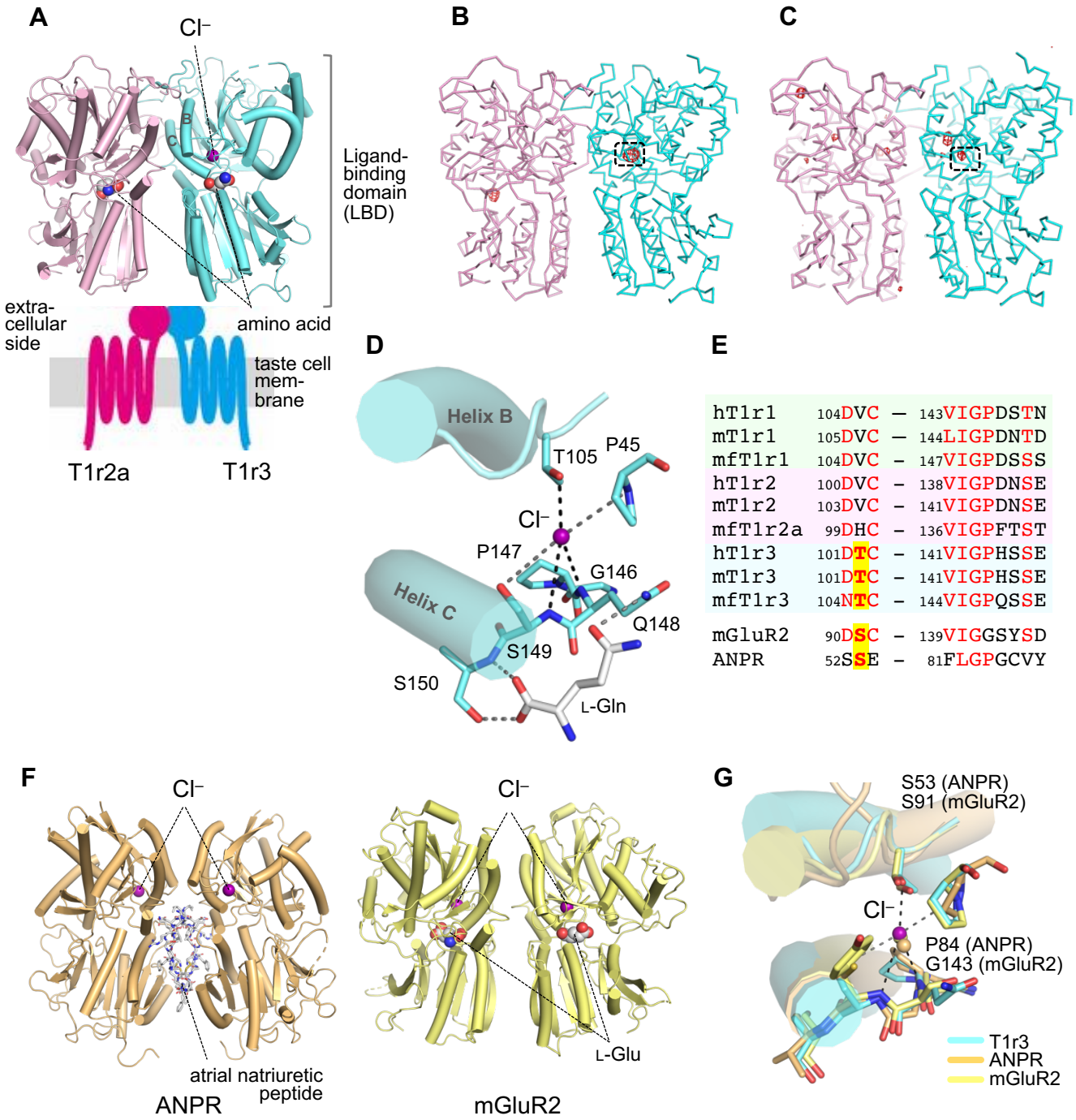

Figure 1. Cl^--binding sites in the medaka fish taste receptor T1r2a/T1r3LBD. (A) Schematic drawing of the overall architecture of T1r2a/T1r3. The crystal structure (PDB ID: 5X2M) is shown at the LBD region, and helices B and C in T1r3 are labeled. (B) Anomalous difference Fourier map (4.5 σ, red) of the Br^--substituted T1r2a/T1r3LBD crystal. (C) Anomalous difference Fourier map (4.5 σ, red) of the Cl^--bound T1r2a/T1r3LBD crystal derived from the diffraction data collected at the wavelength of 2.7 Å. In panels B and C, the site originally identified the Cl^--binding was framed. (D) A close-up view of the Cl^--binding site in T1r3LBD in the Cl^--bound T1r2a/T1r3LBD (PDB ID: 5X2M). (E) Amino-acid sequence alignment of T1r proteins and the related receptors at the Cl^--binding site. The "h," "m," and "mf" prefixes to T1rs indicate human, mouse, and medaka fish, respectively. (F) The structures of ANPR (PDB ID: 1T34, left) (44) and mGluR2 (PDB ID: 5CNI, right) (45) bound with Cl^-. (G) Superposition of the Cl^--binding site in T1r3, ANPR, and mGluR2.

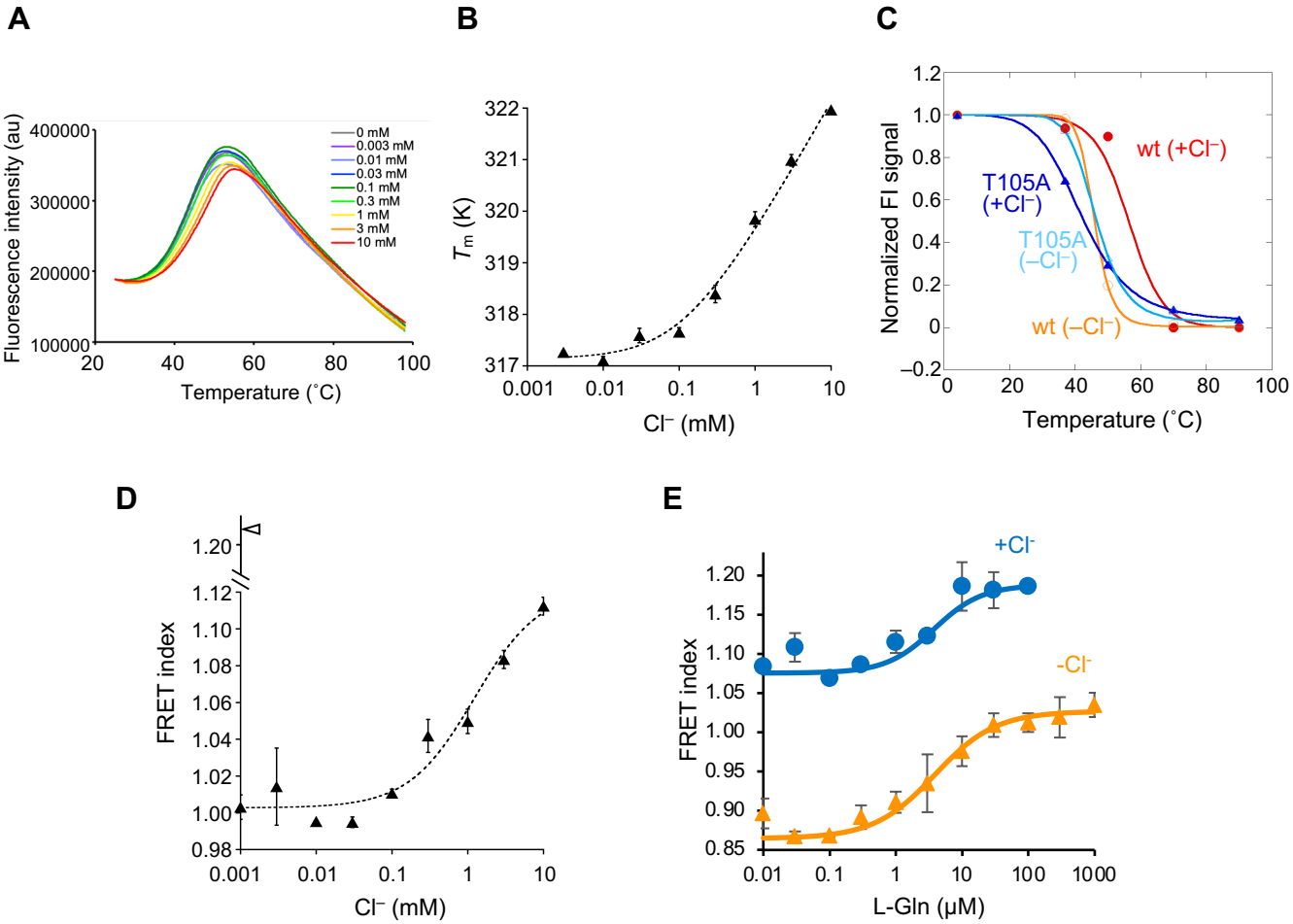

Figure 2. The Cl^--binding properties of T1r2a/T1r3LBD. (A) Thermal melt curves of T1r2a/T1r3LBD in the presence of 0.003 - 10 mM concentrations of Cl^-, measured by DSF. (B) Dose-dependent T_m changes of T1r2a/T1r3LBD by addition of Cl^-. Data points represent mean and s.e.m. (n = 4). (C) Thermal melting curves of wild-type and the T1r3-T105A mutant of T1r2a/T1r3LBD in the presence and absence of Cl^-, analyzed by FSEC-TS. Data points for the wild-type protein represent mean and s.e.m. (n = 3). (D) Dose-dependent FRET signal changes of the T1r2aLBD-Cerulean and T1r3LBD-Venus heterodimer by addition of Cl^-. For comparison, the FRET index for the addition of 1 mM L-glutamine to the same protein sample (1.21 ± 0.003) was shown as an open triangle. (E) Dose-dependent FRET signal changes of the T1r2aLBD-Cerulean and T1r3LBD-Venus heterodimer induced by the addition of L-glutamine in the presence and absence of Cl^-. For panels E and F, data points represent mean and s.e.m. (n = 3).

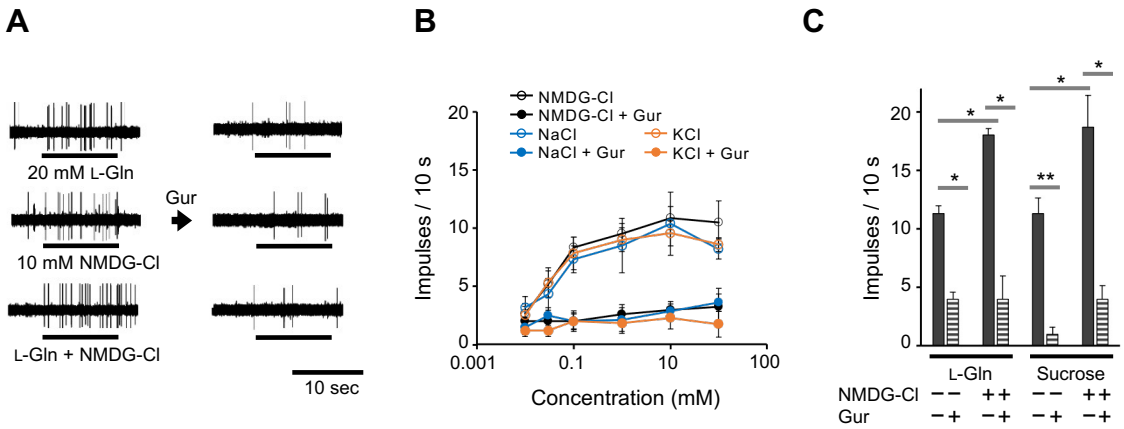

Figure 3. Results of single fiber recordings from the mouse chorda tympani nerve. (A) Representative recordings of sweet-responsive single fibers. The stimuli were 20 mM L-glutamine, 10 mM NMDG-Cl, or 20 mM L-glutamine + 10 mM NMDG-Cl. Lines indicate the application of stimuli to the tongue. After lingual treatment of T1rs blocker, gurmarin (Gur), responses were significantly inhibited. (B) Impulse frequencies in response to the concentration series of NMDG-Cl, NaCl, or KCl before and after Gur treatment. The mean number of net impulses per 10 seconds (mean response) ± s.e.m. in Gur-sensitive fibers (n = 5–6). (C) Impulse frequencies to 20 mM L-glutamine or 100 mM sucrose in the absence or presence of 10 mM NMDG-Cl before and after Gur treatment. Values are mean ± s.e.m. (n = 3). *, **: paired t-test; $P < 0.05$ (*), < 0.01 (**).

Table 1. Properties of the Cl^--binding to T1r2a/T1r3LBD.

Cl^--binding, DSF (n = 4)		
$K_{d\text{-app}}$ (mM)	0.111 ± 0.046	
Protein thermal stability, DSF (n = 6)		
condition	$+Cl^-$	$-Cl^-$
Melting temperature (˚C)	55.2 ± 0.03	46.6 ± 0.06
Protein thermal stability, FSEC-TS		
wild type T1r2a/T1r3LBD (n = 3)		
condition	$+Cl^-$	$-Cl^-$
Melting temperature (˚C)	56.4 ± 5.1	46.0 ± 0.3
mutant T1r2a/T1r3-T105ALBD		
condition	$+Cl^-$	$-Cl^-$
Melting temperature (˚C)	42.7 ± 0.1	46.7 ± 0.7
Cl^-- binding, FRET (n = 3)		
FRET index minimum	1.00 ± 0.005	
FRET index change	0.119 ± 0.014	
EC_{50} (mM)*	1.23 ± 0.53	
L-glutamine binding, FRET (n = 3)		
condition	$+Cl^-$	$-Cl^-$
FRET index minimum	1.08 ± 0.01	0.86 ± 0.01
FRET index change	0.11	0.17
EC_{50} (μM)	3.78 ± 1.29	3.87 ± 1.76
Hill coefficient	1.20 ± 0.88	0.94 ± 0.29
L-glutamine binding, ITC		
condition	$+Cl^-$	$-Cl^-$
N (sites)	0.389 ± 0.028	0.303 ± 0.023
K_a (M^{-1})	$(2.85 \pm 0.65) \times 10^5$	$(2.12 \pm 0.46) \times 10^5$
[converted to K_d (μM)]	[3.51]	[4.72]
ΔH (kcal/mol)	−12.3 ± 1.2	–12.9 ± 1.3
ΔS (cal/mol/deg)	–16.3	−18.8

*Hill coefficient was fixed to 1 for fitting.

Supplementary Information for

Chloride ion evokes taste sensation by binding to the extracellular ligand-binding domain of sweet/umami taste receptors

Nanako Atsumi, Keiko Yasumatsu, Yuriko Takashina, Chiaki Ito, Norihisa Yasui, Atsuko Yamashita

Figures S1 to S2
Tables S1

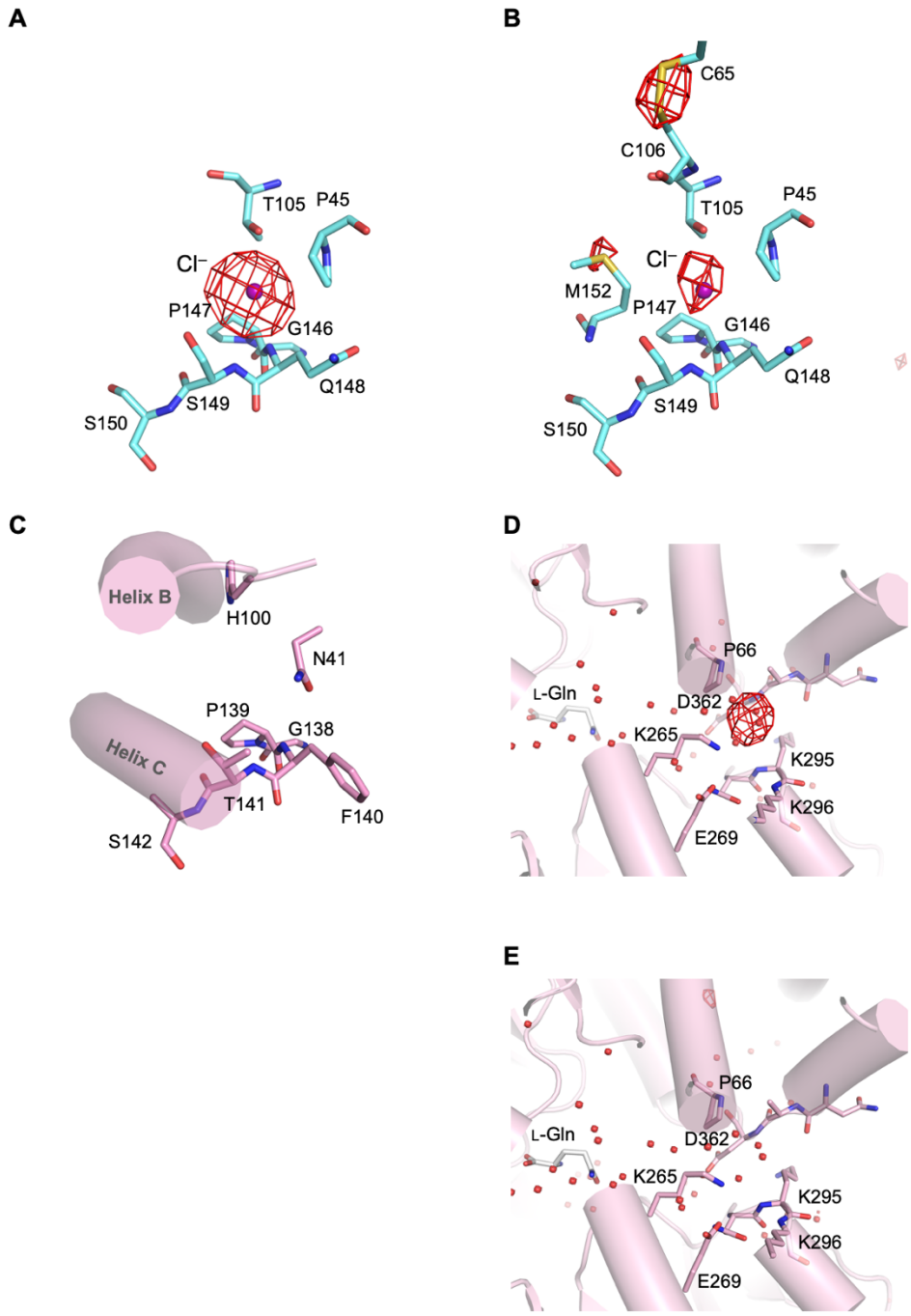

Fig. S1. The structure of the regions relating to the Cl^--binding site in medaka fish T1r2a/T1r3LBD. (A) The Br^--binding site in T1r3. The anomalous difference Fourier map (4.5 σ, red) of the Br^--substituted crystal is overlayed to the Cl^--bound T1r2a/T1r3LBD structure (PDB ID: 5X2M). (B) The Cl^--binding site in T1r3. The anomalous difference Fourier map (4.5 σ, red) calculated from the data collected at the wavelength of 2.7 Å is overlayed. (C) The region in T1r2a, which corresponds to the Cl^--binding site in T1r3, in the Cl^--bound T1r2a/T1r3LBD. (D) The Br^--binding site in T1r2. The anomalous difference Fourier map (4.5 σ, red) is overlayed to the Cl^--bound T1r2a/T1r3LBD structure. (E) The Br^--binding site in T1r2. The 2.7 Å-anomalous difference Fourier map (4.5 σ, red) of the Cl^--bound T1r2a/T1r3LBD, which is the same map shown in panel B, is overlayed to the Br^--binding site in T1r2. No significant peak was observed.

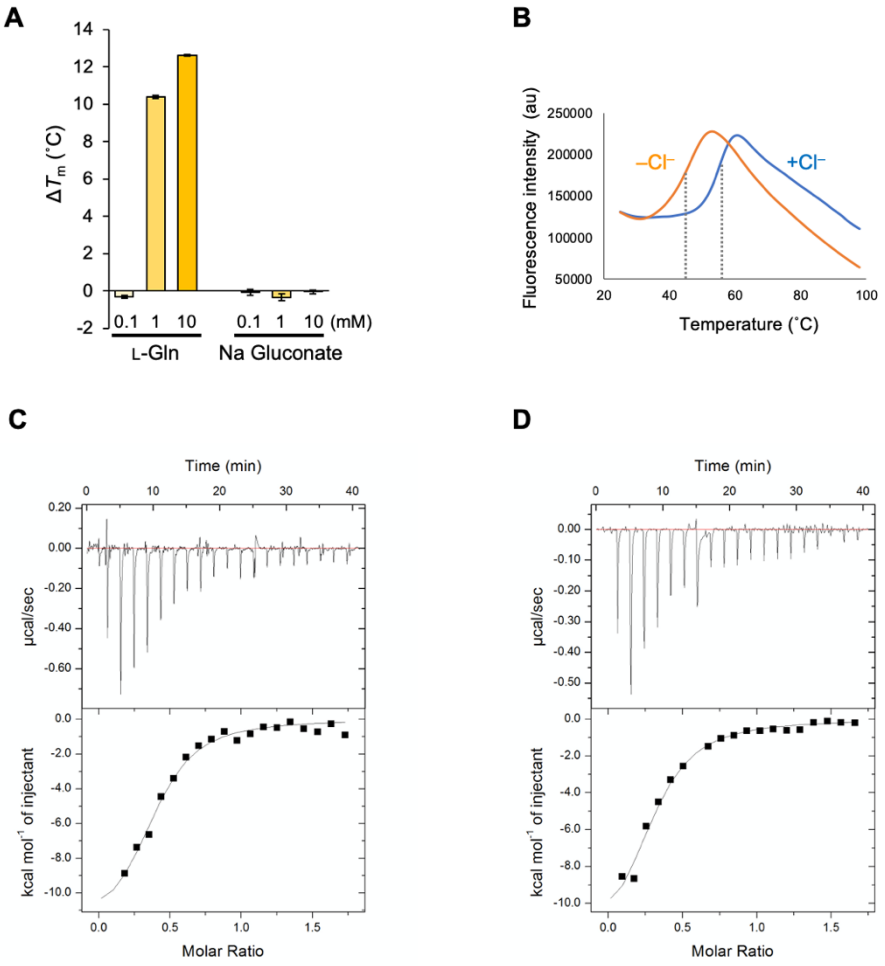

Fig. S2. The properties of T1r2a/T1r3LBD in the presence and absence of Cl^-. (A) Binding analysis of gluconate by DSF. 0.1, 1, and 10 mM of L-glutamine, as a representative ligand, and sodium gluconate was added to T1r2a/T1r3LBD in 20 mM HEPES-NaOH, 300 mM NaCl, pH 7.5. The mean increases of T_m (ΔT_m) from that in the absence of a ligand (54.1 °C, measured on the same sample, n = 2) are plotted. Error bars are in s.e.m. (n = 4). (B) Thermal melt curves of T1r2a/T1r3LBD in the presence or absence of Cl^-, measured by DSF in the same condition in Figure 2C, and the panels C, D in this figure. (C, D) The L-glutamine-binding to T1r2a/T1r3LBD was measured by isothermal titration calorimetry. The upper and lower panels show the raw data and integrated heat signals upon L-glutamine injection to T1r2a/T1r3LBD in the presence (C) and absence (D) of Cl^-. The binding isotherms were fitted assuming 1 ligand: 1 heterodimer binding.

Table S1. X-ray data collection statistics of T1r2a/T1r3LBD-Fab16A complex.

	Br^--bound	**Cl^--bound**
Beamline	SPring-8 BL41XU	Photon Factory BL-1A
Detector	PILATUS6M	EIGER X4M
Wavelength (Å)	0.9194	2.7
Space group	$P2_12_12_1$	$P2_12_12_1$
Cell dimensions		
a (Å)	102.8	102.8
b (Å)	121.6	120.8
c (Å)	129.9	129.1
Resolution (Å)	50-3.41 (3.43-3.41)	49.8-3.32 (3.33-3.32)
R_{sym} (%)*	0.094 (0.808)	0.089 (0.865)
$I/\sigma(I)$ *	16.4 (2.3)	15.1 (2.45)
Completeness (%)*	99.8 (99.2)	99.6 (97.8)
Redundancy*	7.0 (7.0)	6.9 (6.8)

*Values in parentheses refer to data in the highest resolution shells.